Chemical Geology 356 (2013) 181–192

Contents lists available at ScienceDirect

Chemical Geology

journal homepage: www.elsevier.com/locate/chemgeo

Diverse crustal components in pyroxenite xenoliths from Junan, Sulu orogenic belt: Implications for lithospheric modification invoked by continental subduction

Jifeng Ying *, Hongfu Zhang, Yanjie Tang, Benxun Su, Xinhua Zhou

State Key Laboratory of Lithospheric Evolution, Institute of Geology and Geophysics, Chinese Academy of Sciences, Beijing 100029, China

ARTICLE INFO

Article history:
Received 14 December 2012
Received in revised form 5 August 2013
Accepted 6 August 2013
Available online 17 August 2013

Editor: L. Reisberg

Keywords:
Pyroxenite xenoliths
Crustal components
Sulu orogenic belt
Eastern China

ABSTRACT

Detailed mineralogical and geochemical studies have been carried out on a suite of pyroxenite xenoliths captured in a late Mesozoic basaltic dike from Junan, eastern Shandong, which is tectonically situated in the Sulu ultrahigh pressure orogenic belt. Two types of pyroxenites, namely websterite and garnet pyroxenite were identified according to their mineral assemblages. The equilibrium temperatures (828–935 °C) of websterite and garnet pyroxenite xenoliths, falling within the temperature range of lower crustal xenoliths, suggest that they were derived from the lower crust rather than the lithospheric mantle. The websterite xenoliths are characterized by higher MgO and lower Al_2O_3; their convex upward REE patterns, along with lower concentrations of highly incompatible elements indicate that they were high pressure cumulates. Their extremely unradiogenic Nd and radiogenic Sr isotopic compositions imply the contribution of crustal materials to their sources. It is suggested that the precursor melts of websterite xenoliths were derived from a mantle source which had been intensely modified by the subducted lower continental crust of the Yangtze craton following the collision with the North China craton in the Triassic. The compositional features of garnet pyroxenites also suggest their cumulative origin, however, the sharp contrast in trace element concentrations and Sr–Nd isotopic compositions with those of websterite xenoliths indicate they have different precursor melts. Their Sr and Nd isotopic compositions are consistent with the suggestion that their precursor melts were derived from an enriched lithospheric mantle which had been metasomatized by melts released from the Proto-Tethyan oceanic crust which was subducted into the mantle prior to the subduction of continental crust of Yangtze craton. The occurrence of websterite and garnet pyroxenite xenoliths provide evidence that the lithospheric mantle of the North China craton had been significantly modified by the recycled oceanic and continental crust resulting from the collision between the Yangtze craton and the North China craton.

© 2013 Elsevier B.V. All rights reserved.

1. Introduction

Peridotite, granulite, and pyroxenite xenoliths entrained in volcanic rocks have long been used to decipher the physical properties, composition and tectonic evolution of the sub-continental lithosphere. Compared to peridotite and granulite xenoliths, which have relatively definite derivation depths, i.e., peridotite is from the upper mantle and granulite from the lower crust, the issues concerning the depths from which pyroxenites were captured and their petrogenesis are more contentious and not well understood. Pyroxenite may form at lower crustal depths or in the crust–mantle transition zone as evidenced by the occurrence of composite xenoliths consisting of granulites traversed by pyroxenite veins (Upton et al., 2001; Dessai et al., 2004). However, pyroxenite xenoliths have been shown to form largely in the upper mantle and diverse pyroxenites are generally regarded as a physical manifestation of mantle heterogeneity. Different models have been proposed to account for the formation of pyroxenites. They have been suggested to represent primary melt of alkali basaltic or tholeiitic picritic compositions that crystallized within the upper mantle (Ho et al., 2000); high pressure cumulates from basaltic magmas passing through the mantle (Frey, 1980; McGuire and Mukasa, 1997; Litasov et al., 2000; Zhang et al., 2010), and metasomatic products resulting from interaction of reactive melts with mantle peridotites (Garrido and Bodinier, 1999; Liu et al., 2005; Sobolev et al., 2005); or preserved solid-state remnants of subducted oceanic crust (Allegre and Turcotte, 1986; Xu, 2002; Pearson and Nowell, 2004; Yu et al., 2010). In recent years, special attention has been paid to pyroxenites mainly because pyroxenite may act as source rocks for the generation of MORB (Hirschmann and Stolper, 1996) and intra-plate alkali basalts (Carlson and Nowell, 2001; Hirschmann et al., 2003; Kogiso et al., 2003), both of which are traditionally considered to be derived from mantle peridotites.

Peridotite and pyroxenite xenoliths on the North China craton (NCC) frequently occur in Cenozoic alkali basalts, however until recently, because of their lower abundance, pyroxenite xenolith have received

* Corresponding author. Tel.: +86 10 82998532; fax: +86 10 62010846.
E-mail address: jfying@mail.iggcas.ac.cn (J. Ying).

0009-2541/$ – see front matter © 2013 Elsevier B.V. All rights reserved.
http://dx.doi.org/10.1016/j.chemgeo.2013.08.006

less attention than peridotites. Notable progress has been made in recent years with the studies of pyroxenite xenoliths (Xu, 2002; Liu et al., 2005; Yu et al., 2010; Zhang et al., 2010). These results on one hand reconfirmed the diverse origins of pyroxenites; on the other hand, these show us the potential importance of pyroxenites for the understanding of processes in deep lithosphere and regional geodynamics.

In this paper, we report the mineralogical, petrological, elemental and Sr–Nd isotopic compositions of a suite of pyroxenites entrained in a late Mesozoic basaltic dike, eastern Shandong province. These data enable us to put constraints on the origin of diverse pyroxenites and to characterize the recycled continental and oceanic crustal components in the deep lithosphere underneath the Sulu orogenic belt. Moreover, the lithospheric modification of the NCC resulting from northward collision of Yangtze craton is also discussed.

2. Geological background and sample petrography

The NCC, with Archean crustal remnants as old as 3.8 Ga, is one of the oldest cratons in the world (Liu et al., 1992). It is bounded by the Paleozoic central Asian orogenic belt to the north and the Triassic Qinling–Dabie–Sulu ultrahigh pressure metamorphic belt to the south and east, respectively (Fig. 1). The NCC can be divided into Western Block, Eastern Block and Central Orogenic Belt based on geology, tectonic evolution and P–T–t paths of metamorphic basement rocks (Zhao et al., 2001). The basement of the Eastern Block is mainly composed of early to late Archean tonalitic–trondhjemitic–granodioritic (TTG) gneisses and 2.5 Ga syntectonic granitoids. The Western Block consists of late Archean to Paleoproterozoic metasedimentary rocks. The Central Orogenic Belt, separating the Eastern and Western blocks, is composed of late Archean amphibolites, granulites and greenstones overlain by bimodal volcanic rocks and terrigenous sedimentary rocks. It is generally considered that the Eastern and Western blocks evolved independently from late Archean to early Paleoproterozoic times before colliding into a coherent craton along the Central Orogenic Belt at ca. 1.85 Ga (Zhao et al., 2000).

Volcanism on the eastern NCC has been active since the Paleozoic, as manifested by the eruption of Ordovician diamondiferous kimberlites (Chi et al., 1996). After a long magmatic hiatus, magmatism resumed in late Jurassic and accelerated in early Cretaceous and Cenozoic as shown by eruption of voluminous volcanic rocks (Guo et al., 2003; Wu et al., 2005), emplacement of mafic, alkaline and granitoid rocks (Yang et al., 2003; Xu et al., 2004a; Zhang et al., 2005) and extensive Tertiary to Neogene basalts (Zhou and Armstrong, 1982; Cao and Zhu, 1987; Zhi et al., 1990; Zheng et al., 1998).

Shandong Province, situated in the central part of eastern NCC, is separated by the long-lived Tanlu fault into two parts, Luxi in the west and Jiaodong in the east. The tectonics of the Jiaodong region are more complicated than those of Luxi due to the occurrence of the Sulu ultrahigh pressure metamorphic belt which resulted from the continental collision between the NCC and the Yangtze craton in late Triassic.

The Junan xenolith-bearing basaltic dike (latitude: 35°16′28″N, longitude: 118°57′41″E), located around 20 km north of Junan county, Shandong Province, is tectonically situated in the Sulu orogenic belt. This WNW-trending dike intruding a late Mesozoic granite extends up to 200 m with an average width of 10 m. Measurement of the whole rock matrix using the K–Ar method yielded an age of 67 Ma (Ying et al., 2006a). Abundant deep-seated xenoliths including peridotite, granulite and pyroxenite were entrapped within the dike. Detailed investigation of the granulite xenoliths revealed that the lower crust underneath the Sulu orogen has an affinity with the North China craton rather than with the Yangtze craton (Ying et al.,

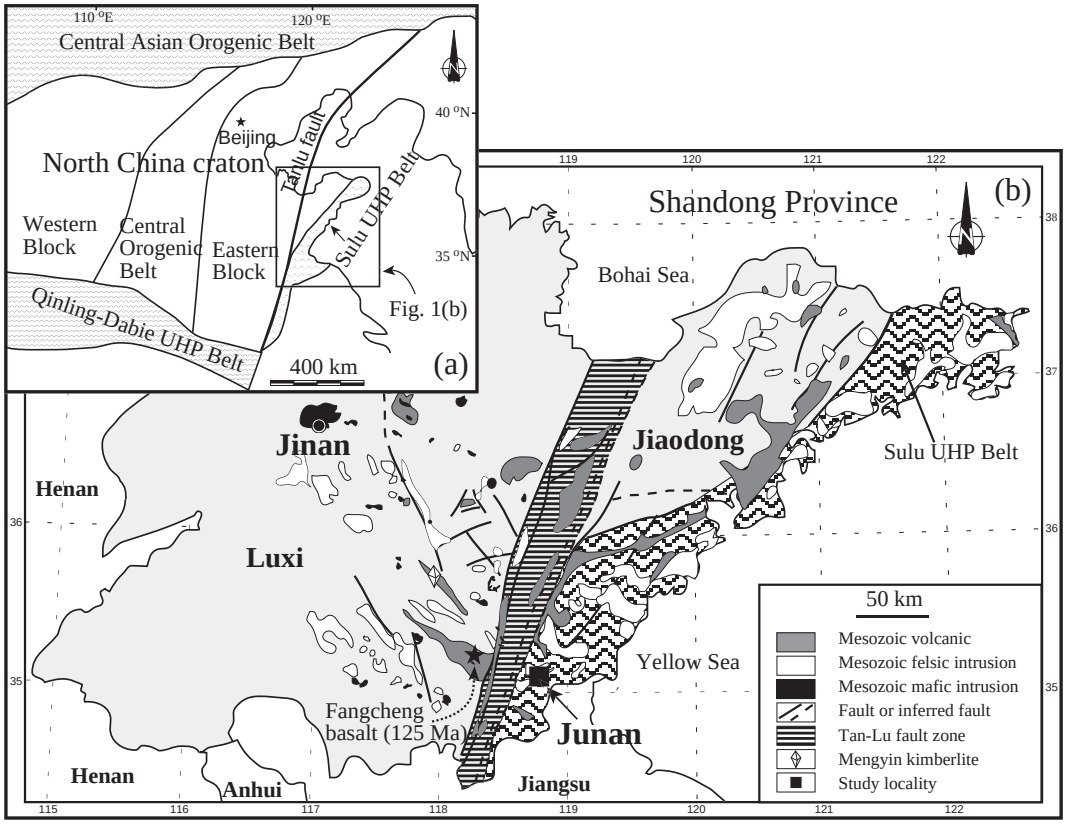

Fig. 1. (a) A schematic map showing the tectonic units surrounding the North China craton (Zhao et al., 2001). The study area, Shandong Province is situated in the eastern part of the North China craton. (b) A geological diagram showing the location of the Junan late Mesozoic dike containing deep-seated xenoliths. Mesozoic extrusive and intrusive rocks, as well as Ordovician Mengyin kimberlite are also shown.
After Zhang et al. (2010).

2010). The studies of peridotite xenoliths demonstrated that the relics of old refractory lithospheric mantle and the newly accreted mantle coexisted in the deep lithosphere (Ying et al., 2006a).

Pyroxenite xenoliths in this study occur as discrete nodules; they are fresh, rounded to sub-angular in shape and range from 3 to 8 cm in size. They are classified into two groups based on their mineral assemblages and compositions. (1) Type 1: websterites. They are spinel-free, and have mineral assemblages of clinopyroxene and orthopyroxene, and are characterized by re-equilibration textures with granoblastic being the most common. They are fine- to medium-grained (1–2 mm). (2) Type 2: garnet pyroxenites. Xenoliths of this group comprise garnet websterite and garnet clinopyroxenite; most of them show granoblastic texture with fine to medium grain sizes (1–2 mm). Garnets and spinels are closely associated and the smaller garnet grains usually occurring along the rims of bigger spinel grains. Garnets usually have kelyphitic rims consisting of fine-grained pyroxene, plagioclase and spinel.

3. Analytical methods

Major element compositions of the constituent minerals were determined with a Cameca SX50 electron microprobe at the Institute of Geology and Geophysics, Chinese Academy of Sciences (IGG). The analyses were operated at 15 kV accelerating voltage, 10 nA current and 2 μm electron beam. Synthetic and natural minerals were utilized as standards. Analytical results of each mineral represent at least 3 point analyses of each grain, and several grains from different parts of each sample. All minerals display intra- and inter-granular homogeneities except that garnets have kelyphitic rims.

Whole rock major oxides were analyzed on the fused glass discs by X-ray fluorescence spectroscopy with an Axios Minerals spectrometer at the IGG. The analytical uncertainties are generally within 1–5%. Loss on ignition (LOI) was determined after the sample powder was heated in a muffle furnace at 1000 °C for 1 h.

For trace element analyses, sample powders were dissolved with distilled HF–HNO_3 in Teflon screw-cap capsules at 180 °C for 7 days, dried and then digested with HNO_3 at 150 °C for 1 day. Dissolved samples were diluted to 50 ml with 1% HNO_3 before analysis. Internal standard In was added to correct matrix effects and instrument drift. Trace element abundances were determined using an inductively coupled plasma mass spectrometer (Finnigan MAT Element) at IGG. Precision and accuracy were evaluated through analyses of Chinese National Standard GSR 3 (basalt powder). Both precision and accuracy are better than 5% for most elements (see Appendix A).

In situ trace element analyses of clinopyroxene and garnet were conducted at IGG, using an Agilent 7500a ICP-MS coupled to an ArF excimer laser ablation system (Geolas Plus). Detailed analytical procedures were described by Gao et al. (2002a). NIST SRM 612 glass standard was used as an external calibration sample (see Appendix A). Data reduction was performed using the GLITTER (Macquarie University) laser ablation software (Griffin et al., 2008).

Sr and Nd isotopic ratios were measured using a GV Isoprobe-T mass spectrometer at IGG. Sample powders were leached with 3N hot HCl

Table 1
Electron microprobe analyses of minerals from Junan pyroxenite xenoliths.

Type 1										
Sample	LG-6		03LG09		05LG53		LG08-11		LG08-12	
Mineral	Cpx	Opx	Cpx	Opx	Cpx	Opx	Cpx	Opx	Cpx	Opx
SiO_2	52.9	54.4	51.1	52.4	51.4	52.9	50.4	52.9	51.0	53.1
TiO_2	0.34	0.14	0.42	0.10	0.49	0.16	0.78	0.17	0.50	0.10
Al_2O_3	2.70	1.59	2.90	1.65	2.91	1.72	5.51	4.05	4.76	3.31
Cr_2O_3	0.22	0.1	0.26	0.11	0.24	0.13	0.33	0.19	0.21	0.14
FeO	7.14	16.5	8.2	20.0	8.68	20.18	6.51	14.3	7.62	16.2
MnO	0.19	0.37	0.18	0.39	0.23	0.41	0.17	0.25	0.15	0.36
MgO	14.7	26.8	13.9	24.6	13.62	23.8	13.9	27.3	13.7	26.2
CaO	20.4	0.68	21.1	0.60	21.6	0.65	21.9	0.53	21.1	0.51
Na_2O	1.08	0.06	0.93	0.02	0.91	0.04	0.88	0.05	1.09	0.05
K_2O	0.00	0.00	0.01	0.01	0.02	0.02	0.00	0.00	0.00	0.00
NiO	0.00	0.00	0.00	0.00	0.00	0.00	0.05	0.08	0.05	0.02
Total	99.6	100.6	99.1	99.9	100.1	100.0	100.3	99.8	100.1	99.9
$Mg^{\#}$	0.79	0.74	0.75	0.69	0.74	0.68	0.79	0.77	0.76	0.74
Wo	0.44	0.01	0.45	0.01	0.46	0.01	0.47	0.01	0.46	0.01
En	0.44	0.73	0.41	0.67	0.40	0.67	0.42	0.76	0.41	0.73
Fs	0.12	0.26	0.14	0.31	0.15	0.32	0.11	0.23	0.13	0.26

Type 2											
Sample	LG08-5				LG08-18				LG08-15		
Mineral	Cpx	Opx	Gt	Sp	Cpx	Opx	Gt	Sp	Cpx	Gt	Sp
SiO_2	49.4	52.1	39.2	0.02	49.5	52.7	39.5	0.05	46.2	38.1	0.03
TiO_2	0.19	0.05	0.04	0.06	0.31	0.03	0.04	0.02	1.48	0.14	0.44
Al_2O_3	7.04	6.27	23.2	59.4	7.44	6.18	23.1	59.6	10.3	21.9	51.9
Cr_2O_3	0.14	0.12	0.16	2.48	0.16	0.10	0.11	1.73	0.02	0.04	0.16
FeO	5.34	11.7	13.9	20.2	5.42	11.5	13.7	19.7	8.40	19.1	34.2
MnO	0.12	0.08	0.42	0.08	0.04	0.13	0.44	0.05	0.03	0.72	0.11
MgO	13.8	28.6	16.1	17.3	13.7	28.5	16.2	17.7	10.5	11.6	11.7
CaO	22.9	0.43	6.50	0.01	22.8	0.33	6.35	0.00	22.1	8.10	0.04
Na_2O	0.62	0.02	0.02	0.01	0.64	0.02	0.04	0.01	1.20	0.01	0.01
K_2O	0.01	0.00	0.00	0.00	0.03	0.01	0.00	0.01	0.00	0.00	0.00
NiO	0.03	0.11	0.03	0.32	0.03	0.04	0.02	0.41	0.01	0.00	0.07
Total	99.6	99.4	99.6	99.9	100.1	99.5	99.5	99.3	100.2	99.7	98.7
$Mg^{\#}$	0.82	0.81	0.67	0.60	0.82	0.82	0.68	0.62	0.69	0.52	0.38
Wo–Py–$Cr^{\#}$	0.50	0.01	0.56	0.03	0.49	0.01	0.56	0.02	0.51	0.41	0.00
En–Alm	0.41	0.81	0.27		0.41	0.81	0.27		0.34	0.38	
Fs–Gro	0.09	0.19	0.16		0.09	0.18	0.16		0.15	0.20	
Spe			0.01				0.01			0.01	

Table 2
Differences in mineral composition of the two types of pyroxenite and peridotite xenoliths.

		Type 1 websterite	Type 2 garnet pyroxenite	Peridotite[a]
cpx	Mg#	0.74–0.79	0.69–0.82	0.86–0.90
	Al_2O_3	2.70–5.51	7.04–10.3	7.22–8.28
opx	Mg#	0.68–0.77	0.81–0.82	0.86–0.89
	Al_2O_3	1.59–4.05	6.18–6.27	4.92–5.94

[a] Peridotite data are from Ying et al. (2006a).

prior to digestion. The acid leached powders spiked with mixed isotopic tracer (^{84}Sr, ^{87}Rb, ^{150}Nd and ^{147}Sm) were dissolved with distilled $HF + HNO_3$ in Savillex Teflon screw-cap beakers at 150 °C for 7 days. The Rb, Sr and REEs were separated from matrix elements with cation exchange columns packed with 2 ml AG50W × 12 resins (200–400 mesh). Subsequently, the Nd and Sm were separated from other REEs using Eichrom-LN columns (Chu et al., 2009). Procedural blanks were <100 pg for Rb, 200 pg for Sr, <20 pg for Sm and <50 pg for Nd, respectively. Measured $^{87}Sr/^{86}Sr$ and $^{143}Nd/^{144}Nd$ ratios were corrected for mass fractionation by normalizing to $^{86}Sr/^{88}Sr = 0.1194$ and $^{146}Nd/^{144}Nd = 0.7219$, respectively. During the period of data collection, the measured values for the JNdi–Nd and NBS987–Sr standards were $^{143}Nd/^{144}Nd = 0.512119 \pm 9$ (n = 8) and $^{87}Sr/^{86}Sr = 0.710247 \pm 7$ (n = 10), respectively.

4. Results

4.1. Mineral major element compositions

Electron microprobe analyses of minerals in the pyroxenite xenoliths are presented in Table 1 and the differences in mineral composition of the two types of pyroxenites are summarized in Table 2.

4.1.1. Pyroxene

Clinopyroxenes from Type 1 xenoliths have much lower Mg# than those from the peridotite xenoliths and Type 2 xenoliths. They have 40–44% En, 11–15% Fs and 44–47 Wo% and fall into the salite region of the pyroxene classification diagram (Fig. 2), while clinopyroxenes from Type 2 xenoliths fall into the diopside region with their 34–41% En, 9–15% Fs and 50–51 Wo%. Orthopyroxenes from Type 1 xenoliths have Mg# ranging from 0.68 to 0.77, and their Al_2O_3 contents varying between 1.59 and 4.05 wt.% are much lower than those of Type 2 xenoliths (Fig. 3).

4.1.2. Spinel

Spinels only occur in Type 2 xenoliths. Their FeO ranges from 19.7 to 34.2 wt.%, Al_2O_3 from 52 to 59 wt.%, and Cr_2O_3 contents are very low (less than 0.03 wt.%).

4.1.3. Garnet

Garnet occurs in Type 2 xenoliths. Garnets from garnet websterites show homogeneous compositions with end-member compositions of 56% pyrope, 27% almandine and 16% grossular, while garnet from garnet clinopyroxenite is more enriched in FeO and CaO, with 41% pyrope, 38% almandine and 20% grossular. Generally, garnets of this study are more enriched in FeO and CaO than those from Hannuoba garnet pyroxenites in northern North China craton (Chen et al., 2001).

4.2. Trace elements of clinopyroxene and garnet

Trace element analyses of clinopyroxene and garnet are provided in electronic Appendix B.

Clinopyroxenes from the two types of xenoliths are quite different both in their absolute trace element concentrations and chondrite-normalized rare earth element patterns. Clinopyroxenes from Type 1 xenoliths exhibit the highest REE concentrations with a total REE of 45–120 ppm. All clinopyroxenes are generally LREE enriched and show convex-up REE pattern which are typical of pyroxene-dominated cumulates (McDonough and Frey, 1989). Sample LG08-11 is distinct from other samples with its much lower LREE concentration. Weak negative Eu anomaly is a common feature for all clinopyroxenes from Type 1 xenoliths (Fig. 4). Clinopyroxenes from Type 2 xenoliths also show convex-up REE pattern, however, their absolute REE concentration is

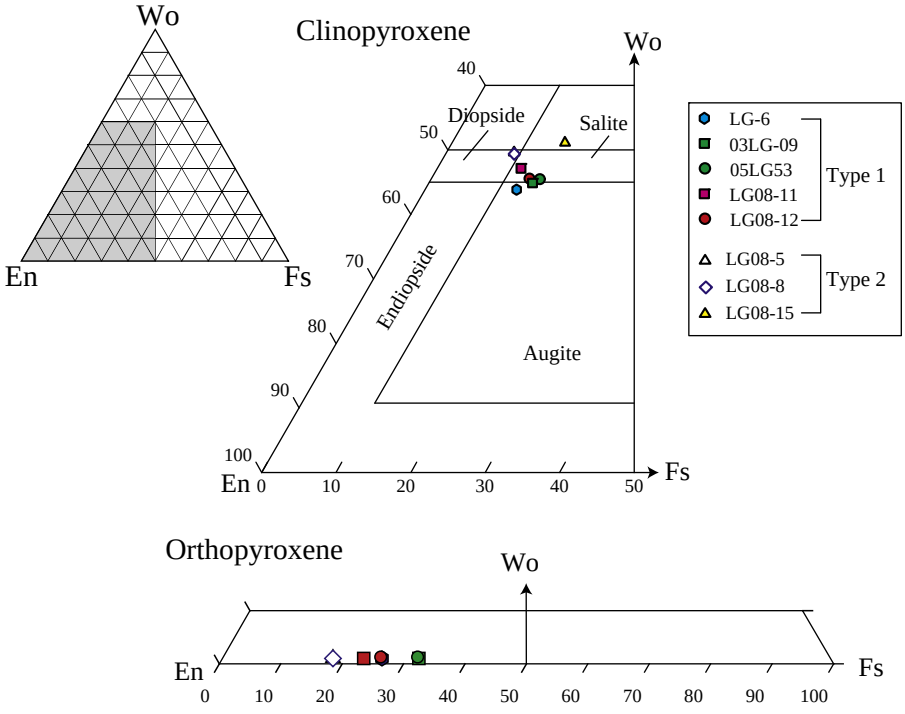

Fig. 2. Mineral compositions of pyroxenes in Junan pyroxenite xenoliths.

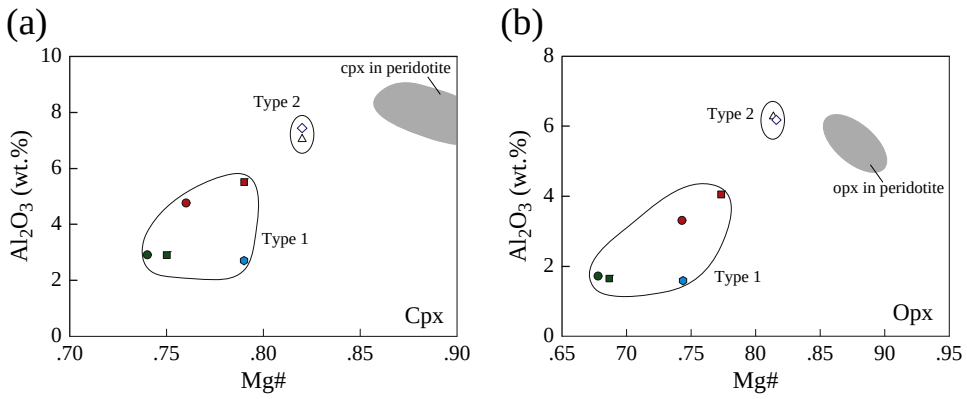

Fig. 3. Al_2O_3 versus Mg# diagrams for clinopyroxenes and orthopyroxenes from Junan pyroxenite xenoliths. Pyroxenes in peridotite xenoliths from Junan basaltic dike are also shown for comparison (Ying et al., 2006a).

about an order of magnitude lower than that of Type 1 xenoliths, and no Eu anomaly was observed.

Garnet in Type 2 xenoliths displays a depleted LREE and enriched HREE pattern (Fig. 4), indicating that the garnet has achieved equilibrium with melts.

4.3. Whole-rock major and trace elements

Major oxide and trace element contents of the pyroxenites are presented in Table 3. The pyroxenites show a wide range in composition (Fig. 5). All samples are characterized by high MgO (15.6–23.4 wt.%) relative to host rock. Type 1 xenoliths have the lowest Al_2O_3 contents of 1.5–4.6 wt.% and the highest FeO of 6.5–14.3 wt.%, while Type 2 xenoliths have higher Al_2O_3 contents of 8.1–12.8 wt.%. It seems that there is no apparent correlation of CaO and SiO_2 contents with the petrographic variations.

Junan pyroxenites exhibit substantial variations in their trace element concentrations (Fig. 6). Type 1 xenoliths are enriched in LREE with $(La/Yb)_N = 2.4–12.1$, their absolute REE concentrations and distribution patterns are similar to those of clinopyroxene, suggesting that clinopyroxene is the dominant reservoir of REE. All samples of this group are characterized by negative Eu anomalies. In primitive mantle normalized spidergram (Fig. 6), all samples display apparent negative HFSE (Nb, Ta, Zr, Hf) and Sr anomalies with the most pronounced negative Nb–Ta and Zr–Hf spikes in 05LG53 and 03LG09. Though depletion of LILE (Rb, Ba) relative to LREE is a common feature for all Type 1 xenoliths, LG08-11 and LG08-12 have much higher concentrations of such elements compared with the others.

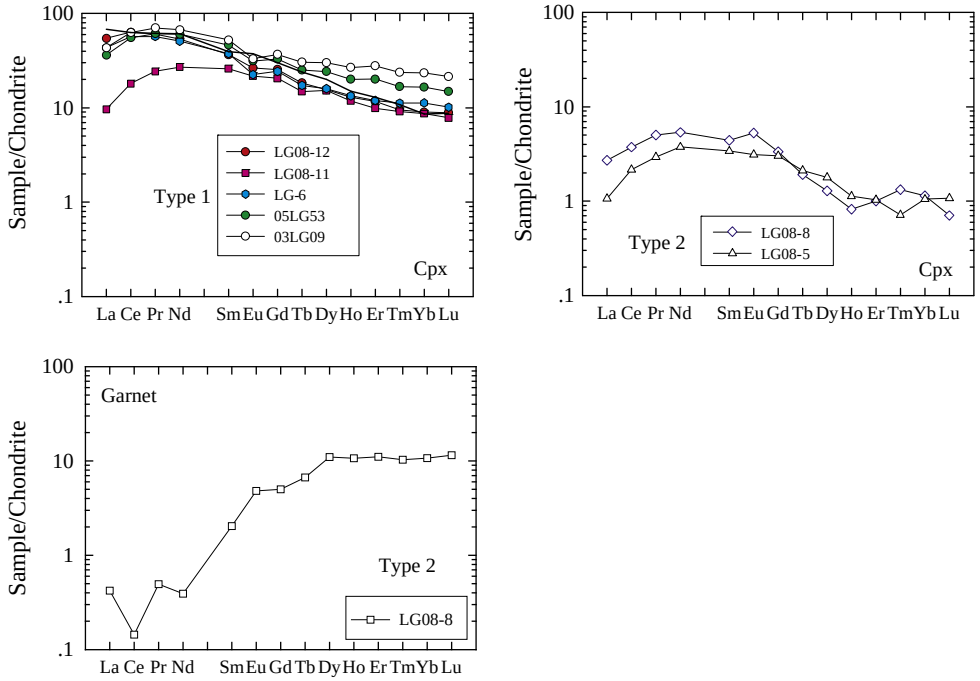

Fig. 4. Chondrite normalized REE patterns for clinopyroxenes and garnet from Junan pyroxenite xenoliths. Chondrite values are from Anders and Grevesse (1989).

Table 3
Bulk-rock major oxides and trace element concentrations of the Junan pyroxenite xenoliths.

	Type 1					Type 2		
	LG-6	03LG09	05LG53	LG08-11[a]	LG08-12	LG08-5	LG08-8[a]	LG08-15[a]
SiO_2	47.9	43.7	44.6	51.8	45.5	44.1	48.3	45.8
TiO_2	0.42	0.44	0.38	0.44	0.57	0.22	0.16	0.12
Al_2O_3	2.03	1.50	1.52	4.71	4.60	8.73	9.78	12.8
TFe_2O_3	12.3	25.3	24.0		12.9	12.1		9.35
MnO	0.22	0.34	0.33	0.21	0.22	0.15	0.09	0.20
MgO	17.1	20.4	20.1	21.3	15.6	18.1	20.8	17.2
CaO	18.2	7.69	8.63	10.1	16.8	15.1	11.0	13.5
Na_2O	1.11	0.15	0.19	0.42	1.16	0.51	0.31	0.32
K_2O	0.03	0.02	0.02	0.00	0.13	0.09	0.02	0.01
P_2O_5	0.03	0.11	0.02		0.10	0.03		
LOI	0.31	0.18	0.14		1.85	0.72		
Total	99.7	99.8	99.9	99.8	99.4	99.9	99.5	99.3
FeO	7.00	14.1	14.3	10.8	6.55	4.00	9.10	
Sc	64.7	45.9	47.8	63.1	68.1	60.5	65.2	54.7
V	164	183	197	228	207	165	164	375
Cr	1474	997	1071	1840	1254	1283	1111	203
Co	39.0	93.2	72.5	61.8	51.9	73.9	73.0	62.7
Ni	110	254	181	402	170	295	305	110
Ga	5.64	9.69	9.76	7.46	9.01	8.59	9.27	18.4
Rb	0.57	0.63	0.38	3.19	3.43	1.61	1.44	7.02
Sr	87.2	37.9	27.9	95.0	129	80.7	55.5	116
Y	18.1	11.7	11.8	14.2	23.3	4.65	4.81	27.8
Zr	59.1	19.6	22.0	27.4	69.5	4.71	6.79	52.2
Nb	1.46	0.24	0.38	2.54	5.53	0.60	1.78	8.44
Cs	0.07	0.09	0.06	0.10	0.25	0.12	0.10	0.19
Ba	5.22	12.6	10.0	52.9	107	45.3	51.2	206
La	10.85	7.60	4.56	4.47	32.0	4.85	3.19	18.6
Ce	30.3	21.2	15.6	11.4	67.0	9.70	7.06	37.7
Pr	4.74	3.30	2.74	1.95	7.78	1.00	0.71	4.66
Nd	21.7	14.6	12.8	10.6	33.2	3.87	3.11	21.1
Sm	4.95	3.23	3.14	3.03	6.33	0.89	0.80	5.18
Eu	1.04	0.71	0.70	0.87	1.64	0.26	0.27	1.63
Gd	4.52	2.86	2.77	3.20	5.99	0.86	0.88	5.28
Tb	0.67	0.44	0.43	0.51	0.83	0.14	0.15	0.83
Dy	3.75	2.37	2.43	3.07	4.47	0.81	0.88	5.22
Ho	0.72	0.47	0.49	0.59	0.89	0.16	0.17	1.10
Er	1.85	1.28	1.33	1.49	2.23	0.40	0.44	2.96
Tm	0.26	0.20	0.20	0.21	0.30	0.05	0.06	0.44
Yb	1.59	1.26	1.29	1.25	1.84	0.31	0.36	2.87
Lu	0.23	0.19	0.20	0.18	0.27	0.05	0.05	0.44
Hf	1.19	0.80	0.94	1.18	1.90	0.22	0.27	1.48
Ta	0.14	0.02	0.03	0.18	0.37	0.04	0.13	0.44
Pb	1.29	0.88	0.97	1.43	2.72	0.92	1.54	1.16
Th	0.17	0.08	0.06	0.26	0.69	0.07	0.19	0.86
U	0.04	0.03	0.03	0.12	0.18	0.04	0.05	0.20

[a] The major oxides of these samples are estimated according to the composition of consisting minerals and their proportions.

Type 2 xenoliths also exhibit enriched LREE patterns with $(La/Yb)_N = 4.5–10.7$. These rocks are Eu anomaly free and show no convex-up REE patterns as their clinopyroxenes do. LG08-15 has a much higher absolute REE concentration than the other two samples. All samples are enriched in LILE and have higher Rb and Ba contents than those of Type 1 xenoliths. Negative Nb–Ta and Zr–Hf anomalies are shown by all samples, positive Pb spikes are also notable for all samples (Fig. 6).

4.4. Whole-rock Sr–Nd isotopes

Sr and Nd data are presented in Table 4 and illustrated in Fig. 7. Junan pyroxenites show an extremely wide range of Sr and Nd isotopic compositions with εNd varying from −1.1 to −28.5 and $^{87}Sr/^{86}Sr$ from 0.7054 to 0.7088. Type 1 xenoliths cluster in the right bottom corner of the Sr–Nd space with the most radiogenic Sr and the least radiogenic Nd isotopic compositions. Type 2 xenoliths show a restricted $^{87}Sr/^{86}Sr$ ratios of 0.70538–0.70545, while their Nd isotopic ratios vary substantially with εNd from −1.1 to −15.3.

5. Discussion

5.1. Estimates of equilibrium conditions for pyroxenite xenoliths

Mineral assemblages can be used to estimate the equilibrium temperature and pressure of the formation for these pyroxenites, as mineral phases in all pyroxenites show equilibrated textures. The two-pyroxene geothermometer of Wells (1977) is used in this paper for temperature estimation and the results are listed in Table 5. The results indicate that the pyroxenites have equilibrated at temperatures of 828–935 °C. We also compared the temperatures of pyroxenites with those of mantle peridotite and lower crust granulite xenoliths entrained in the same host rock. The equilibration temperatures of pyroxenites are similar to those of granulite, and much lower than those of peridotites (Fig. 8). Although it is difficult to calculate the depths at which the pyroxenites were formed,

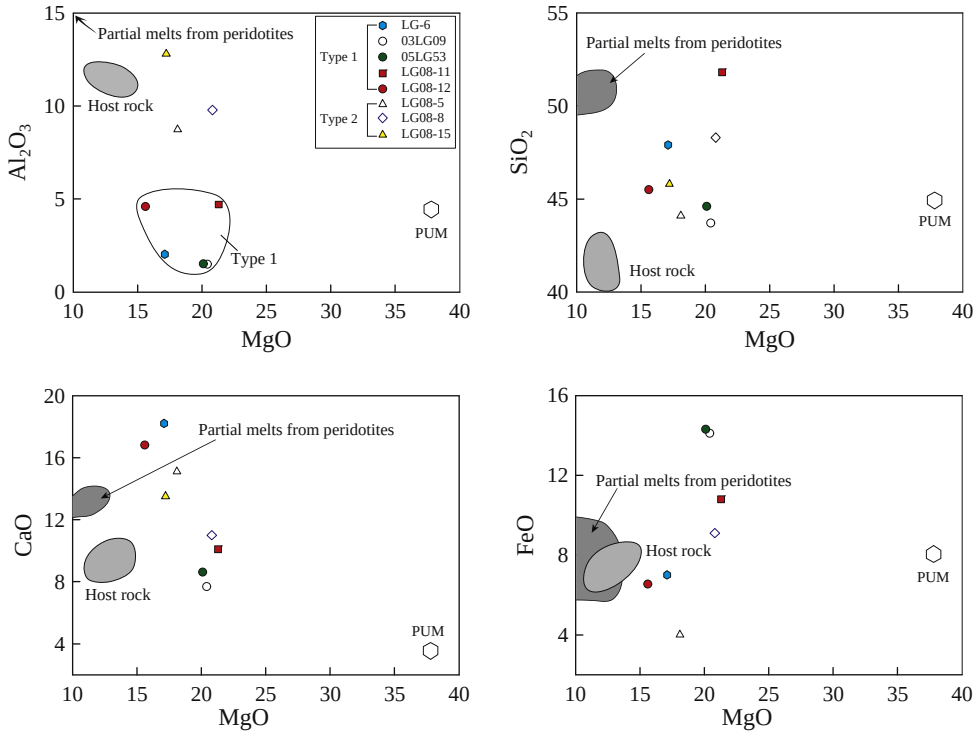

Fig. 5. Major oxides versus MgO diagrams for pyroxenite xenoliths. Host rock (Ying et al. unpublished data), partial melts of peridotites (Falloon et al., 1997) and primitive upper mantle (PUM) (McDonough and Sun, 1995) are shown for comparison.

it can be speculated that the pyroxenites were mainly formed at lower crustal depths assuming that all kinds of xenoliths were equilibrated under the same geothermal conditions.

5.2. Websterite xenoliths: high pressure cumulates of magmas involving subducted continental crust

The petrogenesis of pyroxenite nodules entrained in alkali basalts has long been a controversial issue as we mentioned in the Introduction section, and different models have been proposed to account for their formation. One of the debates concerns whether the pyroxenites represent partial melts of peridotites that have solidified within the mantle (Bodinier et al., 1987; Ho et al., 2000). Many experiments have been performed on peridotites to constrain the compositions of mantle partial melting products (Falloon and Green, 1987; Falloon et al., 1997; Kushiro, 2001). Comparisons of the Type 1 pyroxenites with the partial melts of peridotites produced by experiments reveal that the pyroxenites have much higher MgO and Al_2O_3 contents, and generally lower SiO_2 (Fig. 5). In addition, the convex-up REE patterns exemplified by most of the websterites and depletion of highly incompatible elements are also inconsistent with the geochemical features of partial melts extracted from peridotites. It is thus concluded that the websterite xenoliths are not primary melts or frozen melts from the mantle peridotites.

The convex-up REE patterns shown by most of the websterites and their constituent clinopyroxenes, together with the low abundances of incompatible elements are compelling evidence that the websterites represent fractionally segregated products from magmas under high pressure. As in situ major and trace element analyses of clinopyroxenes have indicated that the clinopyroxenes are homogeneous, implying that they have reached equilibrium with their parental melts, the parental melt compositions can be estimated using the clinopyroxene/basaltic melt partition coefficients. The partition coefficients used in this study are taken from Hart and Dunn (1993), Hauri et al. (1994), and Johnson (1998). In the primitive mantle normalized diagram (Fig. 9), the melts display apparent HFSE depletion, a feature that the host rock is devoid of, therefore, the host basalts can be precluded as the precursor melts of the websterite xenoliths. However, the strongest argument against a link between the websterites and the host basalts comes from the Sr and Nd isotopic compositions. These are quite different from those of MORB, OIB and host basalts, which are thought to be generated from asthenospheric mantle. This implies that the parental magmas of websterites are not from an asthenospheric mantle source.

In general, the trace element distribution patterns of the precursor melts of websterite xenoliths are similar to those of Cretaceous basalts and pyroxenites they bear (Fig. 9) (Zhang et al., 2002; Ying et al., 2006b; Zhang et al., 2007), especially in the aspect of HFSE depletion. It is generally accepted that the depletion of HFSE is a common feature of lavas of active continental margins which suggests that the mantle source had been contaminated by fluids released from subducted slabs (Briqueu et al., 1984; Ringwood, 1990). However, the enriched Sr and Nd isotopic ratios ($^{87}Sr/^{86}Sr$ ratios up to 0.7085 and εNd as low as −29) are inconsistent with those of arc volcanic rocks, precluding an origin of the precursor melts in the mantle wedge. The extremely enriched Sr and Nd isotopic compositions, along with marked HFSE depletion unambiguously require the involvement of continental crust in their mantle sources.

When we compare the Sr–Nd isotopic compositions of websterite xenoliths with those of Cretaceous volcanic rocks and mafic intrusions from southern Shandong (Fig. 7), it is clear that they share a common highly enriched signature. Based on detailed geochemical investigation of Cretaceous extrusive and intrusive rocks, it has been widely accepted that the lithospheric mantle beneath southern Shandong is characterized by extremely enriched Sr and Nd isotopic ratios, and this feature was acquired through extensive interaction with melts derived from the subducted continental crust of the Yangtze craton (Zhang et al., 2002; Xu et al., 2004b; Ying et al., 2006b). However, the discernable discrepancy in Sr and Nd isotopic compositions between the Cretaceous extrusive and intrusive rocks and the websterites suggests that the websterites were not segregated

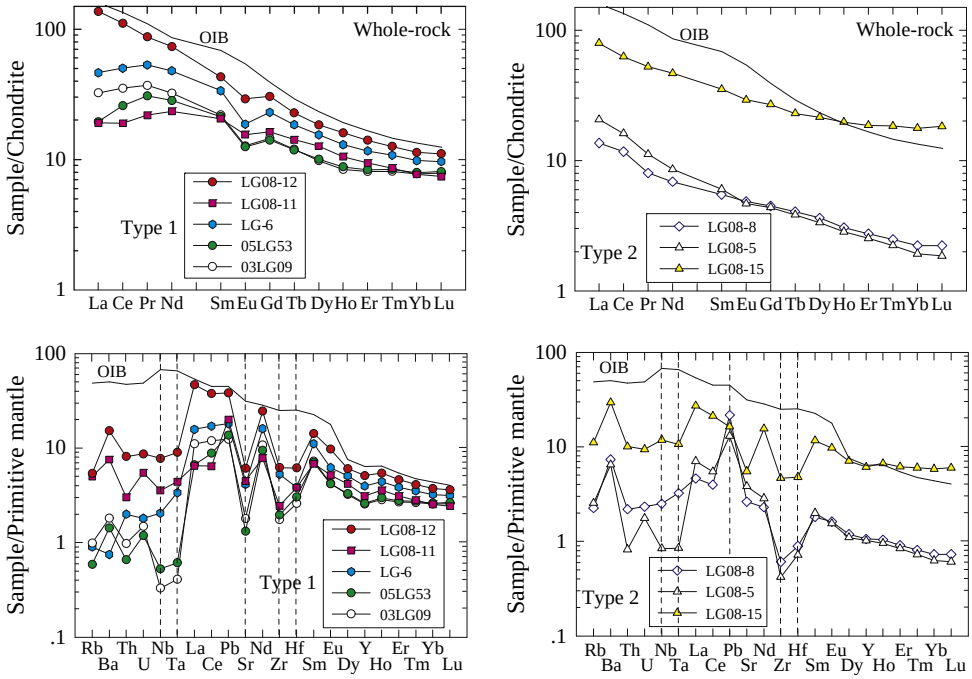

Fig. 6. Chondrite normalized REE patterns and primitive mantle normalized spidergrams of the Junan pyroxenites. Ocean island basalt is from Sun and McDonough (1989). Chondrite and primitive mantle values are from Anders and Grevesse (1989) and Sun and McDonough (1989), respectively.

from those Cretaceous magmas. As equilibrium temperature estimations indicate that the websterites were formed at lower crustal depths, it is reasonable to envisage that the primary magmas from which the websterite fractionally segregated were contaminated by the surrounding lower crust while underplating from the mantle. Such speculation is well supported by the fact that all websterite xenoliths fall into the Sr–Nd isotopic region defined by mixing between the NCC lower crust represented by Junan granulite xenoliths and the enriched lithospheric mantle defined by the Cretaceous basalts.

Alternatively, the thickening and foundering of the NCC lower crust into the mantle resulting from the Triassic collision between the NCC and Yangtze craton might also be a viable mechanism to modify the lithospheric mantle to obtain an enriched isotopic signature (Xu et al., 2008), however, the lower crust beneath Junan has much lower $^{87}Sr/^{86}Sr$ ratios as manifested by the granulite xenoliths, suggesting that the crustal components in websterite xenoliths were unlikely acquired through direct delamination of the NCC lower crust.

Given the similarity in temperature between the granulites and the pyroxenites, possibly suggesting formation at the same depth, we must evaluate the possibility that the websterites were not formed from melts of mantle enriched by continental subduction, but instead represent pyroxenites that have been in the lower crust since Proterozoic or longer. We cannot preclude this possibility on the basis of age as we are not able to obtain age data for the websterites. However, we can consider this issue from their isotopic compositions. The websterites were not cogenetic with the Paleoproterozoic lower crust represented by the Junan granulite xenoliths as they show contrasting Sr–Nd isotopic ratios corrected back to the age of the Junan granulites (Ying et al., 2010). If we presume that the websterites were formed from mantle melts by underplating and intrusion into the lower crust during the Proterozoic, the websterites should show superchondritic initial Nd isotopic ratios, since the mantle in the Proterozoic time is depleted in terms of Sr and Nd isotopes. However, the initial Nd isotopic ratios calculated assuming a Proterozoic formation age (2.0 Ga) are subchondritic ($\varepsilon Nd = -13$ to -28). Therefore, we speculate that it is very unlikely that the websterites have been in the lower crust since Proterozoic or longer.

In summary, the geochemical features of websterite xenoliths argue for their cumulative origin and their formation may have proceeded as the following: subsequent to the collision of the NCC with the Yangtze craton and formation of Dabie–Sulu ultrahigh pressure orogenic belts, the lithospheric mantle of the NCC was intensely metasomatized by the melt derived from the recycled Yangtze lower crust. Magmas derived from partial melting of thus

Table 4
Sr and Nd isotopic compositions of Junan pyroxenite xenoliths.

	Sample	$^{87}Rb/^{86}Sr$	$^{87}Sr/^{86}Sr$	2σ	$^{87}Sr/^{86}Sr_i$[a]	$^{147}Sm/^{144}Nd$	$^{143}Nd/^{144}Nd$	2σ	εNd (t)[a]
Type 1	LG-6	0.2339	0.708844	0.000010	0.708621	0.1408	0.511585	0.000008	−20.5
	03LG09	0.3225	0.708822	0.000010	0.708515	0.1501	0.511179	0.000009	−28.5
	03LG09 dup.		0.708855	0.000014			0.511188	0.000012	
	05LG53	0.0175	0.708824	0.000010	0.708807	0.1432	0.511249	0.000006	−27.1
	LG08-12	0.0477	0.708362	0.000013	0.708317	0.1336	0.511715	0.000006	−18.0
Type 2	LG08-5	0.0411	0.705458	0.000008	0.705419	0.2098	0.512583	0.000011	−1.1
	LG08-8	0.0620	0.705388	0.000008	0.705329	0.1919	0.512150	0.000008	−9.5
	LG08-15	0.1669	0.705394	0.000014	0.705235	0.1644	0.511855	0.000009	−15.3

[a] Initial $^{87}Sr/^{86}Sr$ and eNd(t) are corrected to an age of 67 Ma.

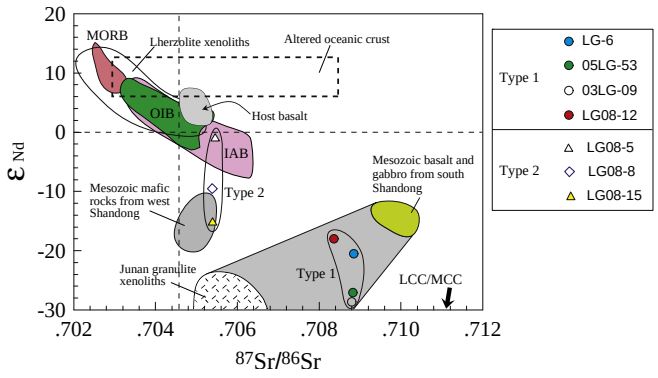

Fig. 7. Sr–Nd correlation diagram for the Junan pyroxenites. MORB, OIB and IAB fields are from Zindler and Hart (1986). Altered oceanic crust is from McCulloch et al. (1980). The isotopic composition of host rock and lherzolite xenoliths are from Ying et.al. (unpublished data). Junan granulite xenoliths are from Ying et al. (2010). Mesozoic mafic rocks from western Shandong are from and Mesozoic basalt and gabbro are from Zhang et al. (2002) and Xu et al. (2004a, 2004b).

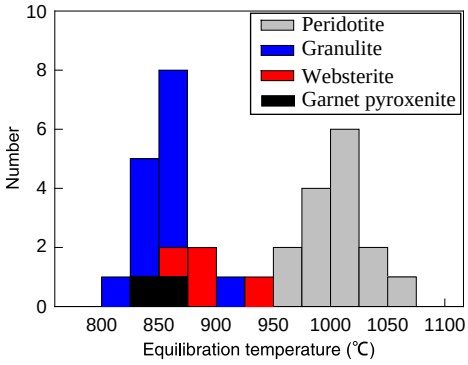

Fig. 8. Equilibrium temperature estimates of pyroxenite, granulite and peridotite xenoliths entrapped in Junan dike.
The granulite and peridotite data are from Ying et al. (2010) and Ying et al. (2006a).

formed enriched mantle source may have been erupted in the Cretaceous as manifested by the Cretaceous basalts. Some magmas may have underplated the NCC lower crust and have been contaminated by the surrounding lower crust material. The websterites were then generated by fractional segregation from such melts.

5.3. Garnet pyroxenites: cumulates of melts with contributions from subducted oceanic crust

Garnet pyroxenites are traditionally interpreted as fractionation products of basaltic magmas in equilibrium with mantle peridotite (Gonzaga et al., 2010), whereas, increasing evidence has shown that garnet pyroxenites may be generated as metasomatic rocks resulting from interaction of reactive fluid and/or melts with mantle peridotites (Mukhopadhyay and Manton, 1994; Garrido and Bodinier, 1999; Liu et al., 2005), or as remnants of recycled oceanic crust or melts derived from such materials (Allegre and Turcotte, 1986; Xu, 2002; Yu et al., 2010).

The equilibrium temperatures of garnet pyroxenites ranging from 828 to 855 °C, are much lower than those of peridotite, but overlap those of granulite xenoliths (Fig. 8). This implies that the garnet pyroxenites were also formed in the lower crust as are the websterites, rather than in the upper mantle. As pyroxenites generated either by reaction between melts and mantle peridotite or by metamorphism of recycled oceanic crust are all derived from the mantle (Allegre and Turcotte, 1986; Liu et al., 2005; Yu et al., 2010), these two models cannot explain the genesis of Junan garnet pyroxenite xenoliths. In addition, the absence of composite xenoliths consisting of peridotite veined by pyroxenite, which is taken as solid petrographic evidence for the metasomatic origin of pyroxenite (Liu et al., 2005) and the lack of positive Sr and Eu anomalies, which are diagnostic of pyroxenites being recycled oceanic crust (Yu et al., 2010) are also not in favor of these two models. Here we proposed that these garnet pyroxenite xenoliths, like the websterite xenoliths, were formed as cumulates, but from different precursor melts. The normal REE pattern of garnet implies that the garnet pyroxenite had been in equilibrium with melts (Fig. 4).

Table 5
Temperature (°C) estimations for Junan pyroxenites.

Sample	T (Wells)
Type 1	
LG-6	935
03LG09	883
05LG53	858
LG08-11	874
LG08-12	895
Type2	
LG08-5	828
LG08-8	855
LG08-15	

The high Mg# and Ni content of Junan garnet pyroxenites are consistent with an origin of their precursor melts in the mantle, however, the sharp contrast in composition with those of websterite xenoliths suggests that their precursor melts are not the same. The calculated hypothetical melts in equilibrium with the garnet pyroxenites have much lower REE concentrations although they are also enriched in LREE relative to HREE. In the primitive mantle normalized diagram, the hypothetical melts are characterized by apparent HFSE depletion, suggesting the involvement of crustal components in their sources (Fig. 9).

The garnet pyroxenites exhibit much lower $^{87}Sr/^{86}Sr$, but higher εNd values than those of websterite xenoliths. As discussed previously, the subducted Yangtze lower continental crust probably played a significant role in the formation of the mantle source for the parental magma to the websterite xenoliths. The unradiogenic $^{87}Sr/^{86}Sr$ and more radiogenic Nd isotopic ratios of the garnet pyroxenites thus preclude the involvement of recycled Yangtze lower continental crust in their mantle sources. Alternatively, subducted oceanic crust may contribute to the formation of mantle sources of parental melts to the garnet pyroxenites.

Geochemical studies of late Mesozoic mafic rocks have revealed that the lithospheric mantle beneath the western Shandong is an aged, enriched mantle with very unradiogenic Nd (εNd as low as −19) coupled with moderately radiogenic Sr (initial $^{87}Sr/^{86}Sr$ ratios around 0.7055), which was inherited from the Archean lithospheric keel (Guo et al., 2003). It has been demonstrated that the altered oceanic crust usually shows a constant Nd isotopic value, but it has a wide range of $^{87}Sr/^{86}Sr$ ratios due to the interaction with sea water (McCulloch et al., 1980). As shown in Fig. 7, the garnet pyroxenites define a mixture between altered oceanic crust and enriched lithospheric mantle represented by the mafic rocks from West Shandong. It is thus likely that the garnet pyroxenites were formed as follows: prior to the Triassic collision between the Yangtze craton and the NCC, the altered Proto-Tethyan oceanic crust was subducted beneath the North China craton, and the initially enriched lithospheric mantle was metasomatized by melts derived from the subducted oceanic crust, which resulted in the formation of the mantle source of garnet pyroxenites. The partial melts derived from the thus formed mantle during post orogenic extension intruded into the lower crust and suffered fractional segregation, which led to the crystallization of garnet pyroxenites. Compared with the highly silicic, LILE and LREE enriched melts

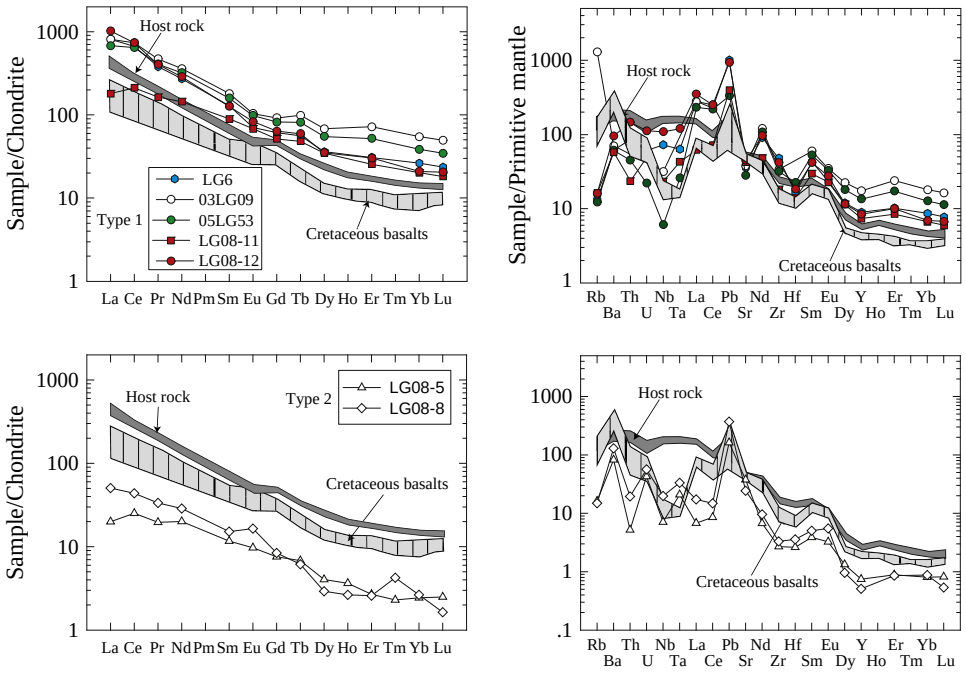

Fig. 9. Chondrite normalized REE patterns and primitive mantle normalized spidergrams of hypothetical melts in equilibrium with pyroxenite xenoliths. Cretaceous basalts from southern Shandong (Zhang et al., 2002) and host basalt (Ying et al. unpublished data) are shown for comparison. Chondrite and primitive mantle values are from Anders and Grevesse (1989) and Sun and McDonough (1989), respectively.

derived from the continental crust, which metasomatized the mantle source of websterite, the oceanic crust derived melts that interacted with the mantle source of garnet pyroxenites which was less enriched in LILE and LREE, and which might explain the trace element differences between the two types of xenoliths.

In terms of this model, the subduction of oceanic crust was followed by the subduction of continental crust. Thus we speculate that the mantle source of the garnet pyroxenites acquired its enriched features much earlier than that of the websterite xenoliths, nevertheless, it is quite difficult to test this hypothesis given the limited dataset.

5.4. Implications for lithospheric modification of the North China craton

It is widely accepted that the initially old, thick and refractory lithospheric mantle beneath the North China craton was replaced by young, thin and fertile mantle in the Mesozoic (Griffin et al., 1998; Menzies and Xu, 1998; Xu, 2001; Gao et al., 2002b; Zheng et al., 2007; Zhang et al., 2009). The collision between the Yangtze craton and the North China craton in the Triassic and the subsequent subduction of Yangtze lower crust is thought to play a vital role in the transformation of the lithospheric mantle, especially in the southern part of the North China craton (Gao et al., 2002b; Zhang et al., 2002, 2003). Detailed geochemical studies of Mesozoic mafic rocks from the southern part of North China craton demonstrated that their highly enriched isotopic signature can only be accounted for by the addition of significant amounts of crustal-derived silicic melts to their source region. The geochemical characteristics of websterite xenoliths in this study reconfirmed the contribution of continental crustal materials in the lithospheric mantle (Zhang et al., 2007, 2010). It is undoubted that there must have been oceanic crustal subduction prior to the continental crust subduction during the amalgamation of the North China craton with the Yangtze craton. However, little evidence had been found so far of this subducted oceanic crust. As we discussed above, the garnet pyroxenite xenoliths of this study may have been derived from a mantle source which had been metasomatized by melts released from the subducted Proto-Tethyan oceanic crust. Therefore, we propose that not only the subducted continental crust but also the recycled oceanic crust played a significant role in modifying the lithospheric mantle of the North China craton.

6. Conclusions

The websterite and garnet pyroxenite xenoliths entrained in the Junan basaltic dike are cumulates that crystallized at lower crustal depths. The precursor melts of websterite xenoliths were derived from a mantle source which may have been intensely modified by the recycled lower continental crust of the Yangtze craton, while the precursor melts of garnet pyroxenite were derived from an enriched lithospheric mantle that may have been metasomatized by melts released from the Proto-Tethyan oceanic crust prior to the subduction of continental crust of Yangtze craton. The occurrences of these pyroxenites provide further evidence that both the subducted continental crust and the recycled oceanic crust during the collision between the North China craton and the Yangtze craton played a significant role in modifying the lithospheric mantle of the North China craton.

Supplementary data to this article can be found online at http://dx.doi.org/10.1016/j.chemgeo.2013.08.006.

Acknowledgments

We are grateful to Q. Mao for assistance with the electron microprobe analysis, H. Li for whole rock and Y.H. Yang for mineral in situ trace element measurements. Thanks are also due to Z.Y. Chu for arranging isotopic analysis. Two anonymous reviewers and the journal editor (Laurie Reisberg) are thanked for their constructive comments and suggestions, which considerately improved the quality of the paper. Financial supports from the Chinese Academy of Sciences (KZCX2-EW-QN106), the Chinese Ministry of Science and Technology

(2009CB825005), and the National Natural Science Foundation of China (91214203, 40973027) are gratefully acknowledged.

References

Allegre, C.J., Turcotte, D.L., 1986. Implications of a two-component marble-cake mantle. Nature 323, 123–127.

Anders, E., Grevesse, N., 1989. Abundances of the elements: meteoritic and solar. Geochim. Cosmochim. Acta 53, 197–214.

Bodinier, J.L., Guiraud, M., Fabries, J., Dostal, J., Dupuy, C., 1987. Petrogenesis of layered pyroxenites from the Lherz, Freychinede and Prades ultramafic bodies (Ariege, French Pyrenees). Geochim. Cosmochim. Acta 51, 279–290.

Briqueu, L., Bougault, H., Joron, J.L., 1984. Quantification of Nb, Ta, Ti and V anomalies in magmas associated with subduction zones: petrogenetic implications. Earth Planet. Sci. Lett. 68, 297–308.

Cao, R.L., Zhu, S.H., 1987. Mantle xenoliths and alkaline rich host rocks in eastern China. In: Nixon, P.N. (Ed.), Mantle Xenoliths. John Wiley & Sons, Chichester, pp. 167–180.

Carlson, R.W., Nowell, G.M., 2001. Olivine-poor sources for mantle-derived magmas: Os and Hf isotopic evidence from potassic magmas of the Colorado Plateau. Geochem. Geophys. Geosyst. 2. http://dx.doi.org/10.1029/2000GC000128.

Chen, S.H., O'Reilly, S.Y., Zhou, X.H., Griffin, W.L., Zhang, G.H., Sun, M., Feng, J.L., Zhang, M., 2001. Thermal and petrological structure of the lithosphere beneath Hannuoba, Sino–Korean craton, China: evidence from xenoliths. Lithos 56, 267–301.

Chi, J.S., Lu, F.X., Zhao, L., 1996. Kimberlites on the North China craton and features of Paleozoic lithospheric mantle. Science Press, Beijing.

Chu, Z., Chen, F., Yang, Y., Guo, J., 2009. Precise determination of Sm, Nd concentrations and Nd isotopic compositions at the nanogram level in geological samples by thermal ionization mass spectrometry. J. Anal. At. Spectrom. 24, 1534–1544.

Dessai, A.G., Markwick, A., Vaselli, O., Downes, H., 2004. Granulite and pyroxenite xenoliths from the Deccan Trap: insight into the nature and composition of the lithosphere beneath cratonic India. Lithos 78, 263–290.

Falloon, T.J., Green, D.H., 1987. Anhydrous partial melting of MORB pyrolite and other peridotite compositions at 10 kbar: implications for the origin of primitive MORB glasses. Mineral. Petrol. 37, 181–219.

Falloon, T.J., Green, D.H., O'Neill, H.S.C., Hibberson, W.O., 1997. Experimental tests of low degree peridotite partial melt compositions: implications for the nature of anhydrous near-solidus peridotite melts at 1 GPa. Earth Planet. Sci. Lett. 152, 149–162.

Frey, F.A., 1980. The origin of pyroxenites and garnet pyroxenites from Salt Lake Crater, Oahu, Hawaii: trace element evidence. Am. J. Sci. 280-A, 427–449.

Gao, S., Liu, X.M., Yuan, H.L., Hattendorf, B., Gunther, D., Chen, L., Hu, S.H., 2002a. Determination of forty two major and trace elements in USGS and NIST SRM glasses by laser ablation-inductively coupled plasma-mass spectrometry. Geostand. Newslett. 26, 181–196.

Gao, S., Rudnick, R.L., Carlson, R.W., McDonough, W.F., Liu, Y.S., 2002b. Re–Os evidence for replacement of ancient mantle lithosphere beneath the North China craton. Earth Planet. Sci. Lett. 198, 307–322.

Garrido, C.J., Bodinier, J.L., 1999. Diversity of mafic rocks in the Ronda peridotite: evidence for pervasive melt–rock reaction during heating of subcontinental lithosphere by upwelling asthenosphere. J. Petrol. 40, 729–754.

Gonzaga, R.G., Lowry, D., Jacob, D.E., LeRoex, A., Schulze, D., Menzies, M.A., 2010. Eclogites and garnet pyroxenites: similarities and differences. J. Volcanol. Geotherm. Res. 190, 235–247.

Griffin, W.L., Zhang, A.D., O'Reilly, S.Y., Ryan, C.G., 1998. Phanerozoic evolution of the lithosphere beneath the Sino–Korean craton. In: Flower, M., Chung, S.L., Lo, C.H., Lee, T.Y. (Eds.), Mantle Dynamics and Plate Interactions in East Asia. Geodynamics series. American Geophysical Union, Washington, DC, pp. 107–126.

Griffin, W., Powell, W., Pearson, N., O'Reilly, S., 2008. GLITTER: data reduction software for laser ablation ICP-MS. In: Sylvester, P. (Ed.), Laser Ablation-ICP-MS in the Earth Sciences. Mineralogical Association of Canada Short Course Series, pp. 204–207.

Guo, F., Fan, W.M., Wang, Y.J., Lin, G., 2003. Geochemistry of late Mesozoic mafic magmatism in west Shandong province, eastern China: characterizing the lost lithospheric mantle beneath the North China Block. Geochem. J. 37, 66–77.

Hart, S.R., Dunn, T., 1993. Experimental CPX/melt partitioning of 24 trace elements. Contrib. Mineral. Petrol. 113, 1–8.

Hauri, E.H., Wagner, T.P., Grove, T.L., 1994. Experimental and natural partitioning of Th, U, Pb and other trace elements between garnet, clinopyroxene and basaltic melts. Chem. Geol. 117, 149–166.

Hirschmann, M.M., Stolper, E.M., 1996. A possible role for garnet pyroxenite in the origin of the "garnet signature" in MORB. Contrib. Mineral. Petrol. 124, 185–208.

Hirschmann, M.M., Kogiso, T., Baker, M.B., Stolper, E.M., 2003. Alkalic magmas generated by partial melting of garnet pyroxenite. Geology 31, 481–484.

Ho, K.-S., Chen, J.-C., Smith, A.D., Juang, W.-S., 2000. Petrogenesis of two groups of pyroxenite from Tungchihsu, Penghu Islands, Taiwan Strait: implications for mantle metasomatism beneath SE China. Chem. Geol. 167, 355–372.

Johnson, K.T.M., 1998. Experimental determination of partition coefficients for rare earth and high-field-strength elements between clinopyroxene, garnet, and basaltic melt at high pressures. Contrib. Mineral. Petrol. 133, 60–68.

Kogiso, T., Hirschmann, M.M., Frost, D.J., 2003. High-pressure partial melting of garnet pyroxenite: possible mafic lithologies in the source of ocean island basalts. Earth Planet. Sci. Lett. 216, 603–617.

Kushiro, I., 2001. Partial melting experiments on peridotite and origin of mid-ocean ridge basalt. Annu. Rev. Earth Planet. Sci. 29, 71–107.

Litasov, K.D., Foley, S.F., Litasov, Y.D., 2000. Magmatic modification and metasomatism of the subcontinental mantle beneath the Vitim volcanic field (East Siberia): evidence from trace element data on pyroxenite and peridotite xenoliths from Miocene picrobasalt. Lithos 54, 83–114.

Liu, D.Y., Nutman, A.P., Compston, W., Wu, J.S., Shen, Q.H., 1992. Remnants of ≥3800 Ma crust in the Chinese part of the Sino–Korean craton. Geology 20, 339–342.

Liu, Y.S., Gao, S., Lee, C.T.A., Hu, S.H., Liu, X.M., Yuan, H.L., 2005. Melt–peridotite interactions: links between garnet pyroxenite and high-Mg# signature of continental crust. Earth Planet. Sci. Lett. 234, 39–57.

McCulloch, M., Grecory, R., Wasserburg, G.J., Taylor, H.P., 1980. A neodymium, strontium, and oxygen isotopic study of the Cretaceous Samail ophiolite and implications for the petrogenesis and sea water–hydrothermal alteration of oceanic crust. Earth Planet. Sci. Lett. 46, 201–211.

McDonough, W.F., Frey, F.A., 1989. Rare earth elements in upper mantle rocks. In: Lipin, B., McKay, G. (Eds.), Geochemistry and Mineralogy of Rare Earth, Elements, pp. 99–145.

McDonough, W.F., Sun, S.s, 1995. The composition of the Earth. Chem. Geol. 120, 223–253.

McGuire, A.V., Mukasa, S.B., 1997. Magmatic modification of the uppermost mantle beneath the Basin and Range to Colorado Plateau Transition Zone; evidence from xenoliths, Wikieup, Arizona. Contrib. Mineral. Petrol. 128, 52–65.

Menzies, M.A., Xu, Y.G., 1998. Geodynamics of the North China craton. In: Flower, M.F.J., Chung, S.L., Lo, C.H., Lee, T.Y. (Eds.), Mantle Dynamics and Plate Interactions in East Asia. Geodynamics Series, 27. American Geophysical Union, pp. 155–165.

Mukhopadhyay, B., Manton, W.I., 1994. Upper-mantle fragments from beneath the Sierra Nevada batholith: partial fusion, fractional crystallization, and metasomatism in a subduction related ancient lithosphere. J. Petrol. 35, 1417–1450.

Pearson, D.G., Nowell, G.M., 2004. Re–Os and Lu–Hf isotope constraints on the origin and age of pyroxenites from the Beni Bousera peridotite massif implications for mixed peridotite–pyroxenite mantle sources. J. Petrol. 45, 439–455.

Ringwood, A.E., 1990. Slab-mantle interactions: 3. Petrogenesis of intraplate magmas and structure of the upper mantle. Chem. Geol. 82, 187–207.

Sobolev, A.V., Hofmann, A.W., Sobolev, S.V., Nikogosian, I.K., 2005. An olivine-free mantle source of Hawaiian shield basalts. Nature 434, 590–597.

Sun, S.S., McDonough, W.F., 1989. Chemical and isotopic systematics of oceanic basalts: implications for mantle composition and processes. In: Saunders, A.D., Norry, M.J. (Eds.), Magmatism in the Oceanic Basalts. Geological Society Special Publication, pp. 313–345.

Upton, B.G.J., Aspen, P., Hinton, R.W., 2001. Pyroxenite and granulite xenoliths from beneath the Scottish Northern Highlands Terrane: evidence for lower-crust/upper-mantle relationships. Contrib. Mineral. Petrol. 142, 178–197.

Wells, P.R.A., 1977. Pyroxene thermometry in simple and complex systems. Contrib. Mineral. Petrol. 62, 129–139.

Wu, F.Y., Lin, J.Q., Wilde, S.A., Zhang, X.O., Yang, J.H., 2005. Nature and significance of the Early Cretaceous giant igneous event in eastern China. Earth Planet. Sci. Lett. 233, 103–119.

Xu, Y.G., 2001. Thermo-tectonic destruction of the Archaean lithospheric keel beneath the Sino–Korean craton in China: evidence, timing and mechanism. Phys. Chem. Earth. 26, 747–757.

Xu, Y.G., 2002. Evidence for crustal components in the mantle and constrains on crustal recycling mechanism: pyroxenite xenoliths from Hanuoba, North China. Chem. Geol. 182, 301–322.

Xu, Y.G., Huang, X.L., Ma, J.L., Wang, Y.B., 2004a. Crust–mantle interaction during the tectono-thermal reactivation of the North China craton: constraints from SHRIMP zircon U–Pb chronology and geochemistry of Mesozoic plutons from western Shandong. Contrib. Mineral. Petrol. 147, 750–767.

Xu, Y.G., Ma, J.L., Huang, X.L., Iizuka, Y., Chung, S.L., Wang, Y.B., Wu, X.Y., 2004b. Early Cretaceous gabbroic complex from Yinan, Shandong Province: petrogenesis and mantle domains beneath the North China craton. Int. J. Earth Sci. 93, 1025–1041.

Xu, W.L., Hergt, J.A., Gao, S., Pei, F.P., Wang, W., Yang, D.B., 2008. Interaction of adakitic melt–peridotite: implications for the high-Mg# signature of Mesozoic adakitic rocks in the eastern North China craton. Earth Planet. Sci. Lett. 265, 123–137.

Yang, J.H., Wu, F.Y., Wilde, S.A., 2003. A review of the geodynamic setting of large-scale late Mesozoic gold mineralization in the North China craton: an association with lithospheric thinning. Ore Geol. Rev. 23, 125–152.

Ying, J.F., Zhang, H.F., Kita, N., Morishita, Y., Shimoda, G., 2006a. Nature and evolution of Late Cretaceous lithospheric mantle beneath the eastern North China craton: constraints from petrology and geochemistry of peridotitic xenoliths from Jünan, Shandong Province, China. Earth Planet. Sci. Lett. 244, 622–638.

Ying, J.F., Zhou, X.H., Zhang, H.F., 2006b. The geochemical variations of mid-Cretaceous lavas across western Shandong Province, China and their tectonic implications. Int. J. Earth Sci. 95, 68–79.

Ying, J.F., Zhang, H.F., Tang, Y.J., 2010. Lower crustal xenoliths from Junan, Shandong province and their bearing on the nature of the lower crust beneath the North China craton. Lithos 119, 363–376.

Yu, S.Y., Xu, Y.G., Ma, J.L., Zheng, Y.F., Kuang, Y.S., Hong, L.B., Ge, W.C., Tong, L.X., 2010. Remnants of oceanic lower crust in the subcontinental lithospheric mantle: trace element and Sr–Nd–O isotope evidence from aluminous garnet pyroxenite xenoliths from Jiaohe, Northeast China. Earth Planet. Sci. Lett. 297, 413–422.

Zhang, H.F., Sun, M., Zhou, X.H., Fan, W.M., Zhai, M.G., Yin, J.F., 2002. Mesozoic lithosphere destruction beneath the North China craton: evidence from major-, trace-element and Sr–Nd–Pb isotope studies of Fangcheng basalts. Contrib. Mineral. Petrol. 144, 241–254.

Zhang, H.F., Sun, M., Zhou, X.H., Zhou, M.F., Fan, W.M., Zheng, J.P., 2003. Secular evolution of the lithosphere beneath the eastern North China craton: evidence from Mesozoic basalts and high-Mg andesites. Geochim. Cosmochim. Acta 67, 4373–4387.

Zhang, H.F., Sun, M., Zhou, X.H., Ying, J.F., 2005. Geochemical constraints on the origin of Mesozoic alkaline intrusive complexes from the North China craton and tectonic implications. Lithos 81, 297–317.

Zhang, H.F., Ying, J.F., Shimoda, G., Kita, N.T., Morishita, Y., Shao, J.A., Tang, Y.J., 2007. Importance of melt circulation and crust–mantle interaction in the lithospheric evolution beneath the North China craton: evidence from Mesozoic basalt-borne clinopyroxene xenocrysts and pyroxenite xenoliths. Lithos 96, 67–89.

Zhang, H.F., Goldstein, S.L., Zhou, X.H., Sun, M., Cai, Y., 2009. Comprehensive refertilization of lithospheric mantle beneath the North China craton: further Os–Sr–Nd isotopic constraints. J. Geol. Soc. 166, 249–259.

Zhang, H.F., Nakamura, E., Kobayashi, K., Ying, J.F., Tang, Y.J., 2010. Recycled crustal melt injection into lithospheric mantle: implication from cumulative composite and pyroxenite xenoliths. Int. J. Earth Sci. 99, 1167–1186.

Zhao, G.C., Cawood, P.A., Wilde, S.A., Sun, M., Lu, L.Z., 2000. Metamorphism of basement rocks in the central zone of the North China craton: implications for Paleoproterozoic tectonic evolution. Precambrian Res. 103, 55–88.

Zhao, G.C., Wilde, S.A., Cawood, P.A., Sun, M., 2001. Archean blocks and their boundaries in the North China craton: lithological, geochemical, structural and P–T path constraints and tectonic evolution. Precambrian Res. 107, 45–73.

Zheng, J.P., O'Reilly, S.Y., Griffin, W.L., Lu, F.X., Zhang, M., 1998. Nature and evolution of Cenozoic lithospheric mantle beneath Shandong peninsula, Sino–Korean craton, eastern China. Int. Geol. Rev. 40, 471–499.

Zheng, J.P., Griffin, W.L., O'Reilly, S.Y., Yu, C.M., Zhang, H.F., Pearson, N., Zhang, M., 2007. Mechanism and timing of lithospheric modification and replacement beneath the eastern North China craton: peridotitic xenoliths from the 100 Ma Fuxin basalts and a regional synthesis. Geochim. Cosmochim. Acta 71, 5203–5225.

Zhi, X.C., Song, Y., Frey, F.A., 1990. Geochemistry of Hannuoba basalts, eastern China: constraints on the origin of continental alkalic and tholeiitic basalt. Chem. Geol. 88, 1–33.

Zhou, X.H., Armstrong, R.L., 1982. Cenozoic volcanic rocks of eastern China — secular and geographic trends in chemistry and strontium isotopic composition. Earth Planet. Sci. Lett. 58, 301–329.

Zindler, A., Hart, S.R., 1986. Chemical geodynamics. Annu. Rev. Earth Planet. Sci. 14, 493–571.